J Membrane Biol (2012) 245:815–826
DOI 10.1007/s00232-012-9484-9

Dielectric Analysis and Multi-cell Electrofusion of the Yeast *Pichia pastoris* for Electrophysiological Studies

Ulrich Terpitz · Sebastian Letschert · Ulrich Bonda · Christoph Spahn · Chonglin Guan · Markus Sauer · Ulrich Zimmermann · Ernst Bamberg · Dirk Zimmermann · Vladimir L. Sukhorukov

Received: 24 April 2012 / Accepted: 30 June 2012 / Published online: 8 August 2012

Abstract The yeast *Pichia pastoris* has become the most favored eukaryotic host for heterologous protein expression. *P. pastoris* strains capable of overexpressing various membrane proteins are now available. Due to their small size and the fungal cell wall, however, *P. pastoris* cells are hardly suitable for direct electrophysiological studies. To overcome these limitations, the present study aimed to produce giant protoplasts of *P. pastoris* by means of multi-cell electrofusion. Using a *P. pastoris* strain expressing channelrhodopsin-2 (ChR2), we first developed an improved enzymatic method for cell wall digestion and preparation of wall-less protoplasts. We thoroughly analyzed the dielectric properties of protoplasts by means of electrorotation and dielectrophoresis. Based on the dielectric data of tiny parental protoplasts (2–4 μm diameter), we elaborated efficient electrofusion conditions yielding consistently stable multinucleated protoplasts of *P. pastoris* with diameters of up to 35 μm. The giant protoplasts were suitable for electrophysiological measurements, as proved by whole-cell patch clamp recordings of light-induced, ChR2-mediated currents, which was impossible with parental protoplasts. The approach presented here offers a potentially valuable technique for the functional analysis of low-signal channels and transporters, expressed heterologously in *P. pastoris* and related host systems.

Keywords Channelrhodopsin-2 · Electrorotation · Dielectrophoresis · Giant protoplast · Cell wall digestion · Patch clamp

U. Terpitz and S. Letschert contributed equally to this work.

Electronic supplementary material The online version of this article (doi:10.1007/s00232-012-9484-9) contains supplementary material, which is available to authorized users.

U. Terpitz · E. Bamberg
Department of Biophysical Chemistry, Max-Planck-Institute of Biophysics, Max-von-Laue-Strasse 3, 60438 Frankfurt, Germany
e-mail: ulrich.terpitz@uni-wuerzburg.de

U. Terpitz · S. Letschert · U. Bonda · C. Spahn · C. Guan · M. Sauer · V. L. Sukhorukov (✉)
Department of Biotechnology and Biophysics, Julius-Maximilians-University Würzburg, Biozentrum-Am Hubland, 97074 Würzburg, Germany
e-mail: sukhorukov@biozentrum.uni-wuerzburg.de

U. Zimmermann
ZIM Plant Technology, Neuendorfstr. 19, 16761 Hennigsdorf, Germany

E. Bamberg · D. Zimmermann
Department of Biochemistry, Chemistry and Pharmacy, Johann-Wolfgang-Goethe University Frankfurt, Max-von-Laue-Strasse 1, 60438 Frankfurt, Germany

Introduction

The methylotrophic yeast *Pichia pastoris* is currently the most widely used yeast species in the production of recombinant proteins for research and biotechnological applications (Macauley-Patrick et al. 2005; De Schutter et al. 2009). *P. pastoris* is easy to manipulate genetically (Daly and Hearn 2005). It grows to high cell densities and provides strong promoters for transgene expression, such as the methanol-inducible alcohol oxidase 1 (AOX1) promoter (Tschopp et al. 1987). In general, *P. pastoris* enables large-scale production of recombinant proteins at a much lower cost than most other eukaryotic systems (Bretthauer and Castellino 1999).

Besides soluble proteins, a range of recombinant membrane proteins, including ion channels and transporters (e.g., channelrhodopsin-2, ChR2), can be efficiently expressed in *P. pastoris* (Diatloff et al. 2006; Bamann et al. 2008). Unfortunately, direct electrophysiological analysis of these channels is experimentally cumbersome, if not impossible, because of the dense fungal cell wall and small size of *P. pastoris* cells (2–4 μm diameter). Therefore, studies of membrane proteins in *P. pastoris* cells by the patch clamp technique require enzymatic removal of the cell wall and subsequent enlargement of the isolated wall-less protoplasts.

Recently, stable giant HEK293 cells and giant protoplasts of the baker yeast *Saccharomyces cerevisiae* with diameters of up to 50–65 μm have been successfully generated by multi-cell electrofusion (Terpitz et al. 2008; Zimmermann et al. 2006). In view of the outlined advantages of *P. pastoris* over other eukaryotic hosts for recombinant protein expression, the ultimate aim of the present study was to make this yeast species accessible to the patch clamp technique. Here, we report the production of "patchable" giant *P. pastoris* protoplasts by means of multi-cell electrofusion.

The electrofusion technique combines the creation of tight contacts between cell membranes by dielectrophoretic alignment and the electric membrane breakdown in the contact zones to initiate cell fusion (Zimmermann and Neil 1996). To achieve maximal efficiency of electrofusion, several critical issues concerning both isolation and electromanipulation of protoplasts had to be addressed within this study. Prior to electrofusion, we developed an improved method for cell wall digestion and isolation of wall-less protoplasts from *P. pastoris* expressing ChR2. This was necessary because of the methanol-mediated resistance of the yeast cell wall to mycolytic enzymes. We also analyzed the dielectric properties of *P. pastoris* cells and protoplasts by two complementary AC electrokinetic techniques, electrorotation (ROT) and dielectrophoresis (DEP).

Based on the dielectric data of parental protoplasts, we elaborated efficient electrofusion conditions concerning the AC field frequency for stable cell alignment, field strength and duration of breakdown pulses triggering membrane fusion. The optimized electrofusion protocol consistently yielded stable multinuclear *P. pastoris* protoplasts with diameters of up to ~35 μm. The electrofused giant protoplasts were suitable for electrophysiological measurements, as proved by application of the whole-cell patch clamp technique and recordings of light-induced currents mediated by ChR2. Compared to tiny parental protoplasts, the strongly enlarged plasma membrane area of giant protoplasts greatly increased the amount of electrically accessible membrane proteins, thus enabling patch clamp studies of low-signal channels and transporters.

Materials and Methods

Yeast Cell Culture, ChR2-YFP Expression and Protoplast Isolation

The yeast strains used here were *P. pastoris* SMD1163 (Daly and Hearn 2005) and transformed *P. pastoris* expressing channelrhodopsin-2(C128T)-YFP (ChR2-YFP) (Bamann et al. 2008), hereafter referred to as wild-type (wt) and ChR2 cells, respectively. Cells were grown on YPD agar plates (1 % yeast extract, 2 % peptone, 2 % glucose) at 30 °C. Prior to protoplast isolation, plated cells were transferred to and grown in liquid BMGY medium for 8 h (transformed cells) or 17–20 h (control). AOX1 promoter-controlled protein expression was initiated by transferring an aliquot of BMGY-yeast suspension to methanol-containing BMMY medium supplemented with 1 μM all-*trans*-retinal (Sigma, Taufkirchen, Germany). Cells were then grown in 250-ml 3-baffle flasks (Schott-Duran, Mainz, Germany) at 30 °C, 140 rpm, for ~36 h to 0.8–1.2 OD_{600nm}. The use of baffled flasks significantly enhanced the expression of ChR2-YFP (see Supplemental Fig. S1). Protein expression was examined by fluorescence microscopy (Axiovert 25 from Carl Zeiss, Jena, Germany, and TCS from Leica, Wetzlar, Germany) and by flow cytometry (FACS Calibur from Becton–Dickinson, San Jose, CA) (Supplemental Fig. S1). Heat inactivation was achieved by autoclaving the cells in water at 121 °C for 20 min.

For isolation of wall-less protoplasts, ~10^8 cells were harvested by centrifugation (1,500×*g*, 5 min) from liquid culture. Cells were washed first in 5 ml H_2O and then in 5 ml SED buffer, containing 1 M sorbitol, 25 mM EDTA and 50 mM 2-dithiotheritol (DTT) (Cregg et al. 1985). Digestion of the cell wall was performed for 5 h at 30 °C and 140 rpm in stabilizing buffer (0.7 M magnesium sulfate and 50 mM Tris, pH 7.5) with a modified enzyme cocktail containing 100 μg/ml zymolyase 100T (Seikagaku, Tokyo, Japan), 50 μl Glusulase (from *Helix pomatia*; PerkinElmer, Boston, MA), 2 mg/ml Glucanex (Sigma, Steinheim, Germany), 1 μg/ml ergosterol, 2 mM DTT and 1 μM all-*trans*-retinal (Klinner et al. 1980). Glucanex was obsolete when cells were grown in methanol-free medium (see below).

Expression of ChR2(C128T)-YFP in *P. pastoris* cells reached its maximum within 48 h in methanol-containing BMMY medium (Supplemental Fig. S1). A side effect of methanol, however, was an increased resistance of the cell wall to zymolyase degradation, which can be explained by the methanol-mediated changes in cell wall morphology reported elsewhere (Canales et al. 1998). To overcome this problem, we supplemented the enzyme cocktail with Glucanex, an enzyme exhibiting beta-1,3 and

beta-1,6-glucanase activity. The optimized enzyme mixture completely digested the cell wall of Chr2(C128T)-YFP-expressing yeast cells, thus yielding "naked" protoplasts with high protein expression (Fig. 1c). Wall-less protoplasts could be easily distinguished from intact cells by their ideal spherical shape and lack of calcofluor white staining, as proven by fluorescence microscopy (Fig. 1b vs. a).

Electrorotation and Dielectrophoresis Spectra

ROT and DEP spectra were measured in four-electrode microchambers arranged as planar arrays of circular electrodes of 100 µm (ROT) or 60 µm (DEP) diameter, 140 nm thickness and 300 µm (ROT) and 100 µm (DEP) electrode spacing (Kiesel et al. 2006). To generate rotating fields, the electrodes were driven by four 90° phase-shifted signals from a pulse generator (HP 8130A; Hewlett-Packard, Boeblingen, Germany) with ~2.0–4.5 V_{PP} amplitude over a frequency range from ~1 kHz to 150 MHz. For DEP measurements, two neighboring electrodes were short-circuited and the opposite pairs of shorted electrodes were driven by two 180° phase-shifted signals up to 300 MHz. A sample of cell or protoplast suspension (25 µl, ~10^5 cells/ml) was pipetted onto the microchamber and covered with a glass coverslip. Cells were observed using a BX 50 Olympus microscope (Hamburg, Germany) equipped with a CCD video camera. Cell radii were determined with a calibrated ocular micrometer. ROT spectra were monitored by decreasing the field frequency in steps. At each frequency, the ROT speed, Ω (radian/s), of lone cells located near the center of the chamber was measured using a stopwatch. ROT spectra were normalized to a field strength of 100 V/cm.

In separate experiments, the field frequencies (f_{c1}) that induced the fastest antifield cell rotation were also determined by the contrarotating field (CRF) technique (Arnold and Zimmermann 1988). CRF data were used for determination of the plasma membrane capacitance (C_m) and conductance (G_m) in large cell samples.

During DEP measurements, two crossover frequencies, f_{d1} and f_{d2}, of the spectrum were determined as a function of external conductivity, σ_e, by adjusting the field frequency to the value at which the DEP force is zero (i.e., no cell movement toward or away from the electrode edges occurred). The DEP response of 5–10 cells was measured in each experiment. Medium conductivity, σ_e, was varied between ~1 and 1,000 mS/m by adding increasing amounts of calcium acetate and magnesium acetate (in a ratio of 1:5). Osmolarity was adjusted with sorbitol to 500 mosmol (intact cells) and 650 mosmol (protoplasts). To avoid ion loss from the cytosol, cells and protoplasts were stored on ice during ROT and DEP measurements. At conductivities >100 mS/m, a denser sucrose solution was used instead of sorbitol in order to slow down sedimentation and to prevent adhesion of cells to the glass bottom of the chamber.

Multi-cell Electrofusion: Equipment and Procedure

Based on earlier reports (Terpitz et al. 2008; Zimmermann et al. 2006; Sukhorukov et al. 2006) and the new dielectric

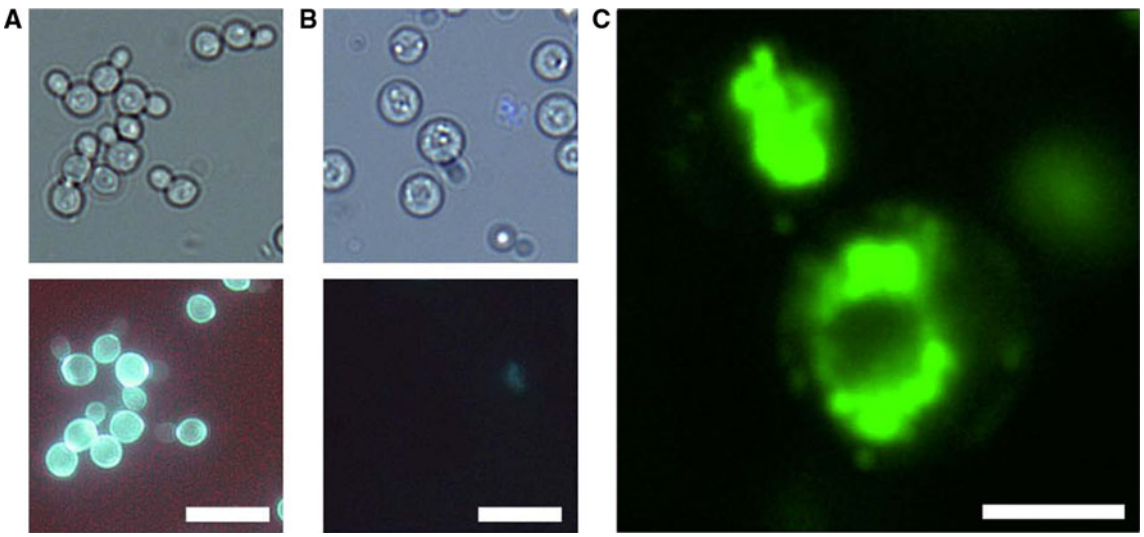

Fig. 1 Bright-field and fluorescence microphotographs of walled *P. pastoris* cells (**a**) and of isolated protoplasts (**b**). Unlike intact cells, protoplasts exhibited an ideal spherical shape and a lack of calcofluor white staining (**b**, *bottom*), suggesting complete cell wall digestion. **c** Typical ChR2(C128T)-YFP expression pattern in *Pichia* cells revealed by confocal laser scanning microscopy. Apparently, YFP was mainly expressed in the cytosolic vesicles and to a much lesser extent in the plasma membrane. *White bars* = 10 µm (**a**, **b**) and 2 µm (**c**)

data obtained in the present study, an optimized protocol for production of giant *P. pastoris* protoplasts via multicell electrofusion was developed. Freshly isolated protoplasts were washed twice with and resuspended (1,000×*g*, 5 min, 4 °C) in low-ionic electrofusion medium containing 0.8 M sorbitol, 0.5 mM Mg acetate and 0.1 mM Ca acetate (conductivity $\sigma \approx 8$ mS/m) at a density of $\sim 5 \times 10^5$ cells/µl. Protoplasts were stored on ice and used for experiments within 4 h after isolation.

For electrofusion, 2–3 µl of protoplast suspension was transferred into the fusion chamber consisting of two parallel cylindrical, stainless-steel electrodes (200 µm diameter) mounted on a glass substrate at a distance of 200 µm. The electric field was delivered from a programmable arbitrary waveform generator (AT-AWG 2000; Acquitek, Massy, France), amplified with a high-voltage amplifier (A400DI; FLC Electronics, Partille, Sweden) and fed to the electrodes of the fusion chamber. Protoplasts were first collected and aligned into chains by dielectrophoresis in an AC field of 2 MHz frequency and 800 V/cm intensity, applied for 20 s. Membrane fusion was initiated by four rectangular DC pulses of 8–10 kV/cm amplitude and 22 µs duration. The time interval between consecutive pulses was 100 ms. Before and after each DC pulse, the alignment AC field and, thus, the DEP force was switched off for 1 µs. After the final DC pulse, a 2-MHz field of 400 V/cm amplitude was applied for a further 30 s in order to keep the fusing protoplasts in close contact. After electromanipulation, protoplasts were left without disturbance for about 2 min.

Patch Clamp

Patch clamp experiments were performed as described in detail before (Terpitz et al. 2008). Current recordings were performed in the whole-cell configuration in voltage-clamp mode. Pipettes (GB150F-8P, Scientific-Instruments, Hofheim, Germany) with a tip opening diameter of 1 µm exhibited a resistance of 5–8 MΩ in sealing buffer. Stray capacitance (9.2 ± 0.4 pF, $n = 6$) and the whole-cell capacitance of protoplasts were determined from charge transfer recorded after application of a voltage step. Capacitance was determined from the slope of the linear fit to the ΔQ/ΔV data. The membrane area was calculated from the measured diameter by assuming spherical geometry. Pipette solution contained 110 mM KCl, 10 mM EGTA, 5 mM $MgCl_2$. The sealing buffer and bath solution contained 140 mM NaCl, 5 mM $MgCl_2$, 10 mM $CaCl_2$. High calcium concentration enabled stable gigaseal formation (Priel et al. 2007). All buffers were complemented with 10 mM HEPES, pH 7.4 (pipette and sealing buffer) or pH 5.2 (bath solution), and osmotically adjusted to 700 mosmol/kg (Knauer, Berlin-Zehlendorf, Germany) with sorbitol.

Results and Discussion

Electrorotation and Dielectrophoresis of Cells and Protoplasts

Prompted by the observation that overexpression of ChR2 in human cells (HEK293 line) (Zimmermann et al. 2008) significantly increased the area-specific membrane capacitance (C_m), we first analyzed the impact of ChR2 expression on the dielectric properties of *P. pastoris*. To this end we examined the AC electrokinetic behavior of walled *P. pastoris* cells and isolated protoplasts over wide ranges of field frequency (~ 1 kHz $< f <$ 150 MHz) and medium conductivity (1 mS/m $< \sigma_e <$ ~ 1 S/m), using two complementary techniques, ROT and DEP. Figure 2a, b show, respectively, the ROT spectra of ChR2-expressing protoplasts and cells, taken at various conductivities (σ_e) of suspending medium. The ROT spectra of wild-type protoplasts/cells were very similar to those shown in Fig. 2, obtained with ChR2-expressing samples.

Consistent with the single-shell model (SSM) (Jones 1995; Gimsa et al. 1996; Pethig 2010), the ROT spectra of protoplasts could be fitted very accurately by a superposition of two Lorentzian functions (curves in Fig. 2a). The two ROT peaks are indicated by the characteristic frequencies f_{c1} and f_{c2}, for the antifield and cofield rotations, respectively. Unlike isolated protoplasts, walled *P. pastoris* cells exhibited an additional cofield shoulder (arrow in Fig. 2b) at the lowest conductivity ($\sigma_e = 1$ mS/m) and a broad antifield rotation peak at higher conductivities (165–330 mS/m). These deviations from the SSM indicate at least one additional dielectric relaxation, caused most likely by the yeast cell wall (see below, the double-shell model, DSM). As seen in Fig. 3a, c, enzymatic digestion of the cell wall also gave rise to a marked shift of the antifield f_{c1} peak to lower frequencies at conductivities σ_e below ~ 10 mS/m, without significantly affecting the position of the cofield ROT peak f_{c2} ($\sim$60–100 MHz).

The influence of the cell wall is even more evident from the DEP data shown in Fig. 3b, d, which illustrate the conductivity dependence of the DEP crossover frequencies ($f_{d1,d2}$) for protoplasts and cells, respectively. The $f_{d1,2}$ data points indicate transitions between positive and negative DEP as a function of external conductivity, σ_e. As seen in

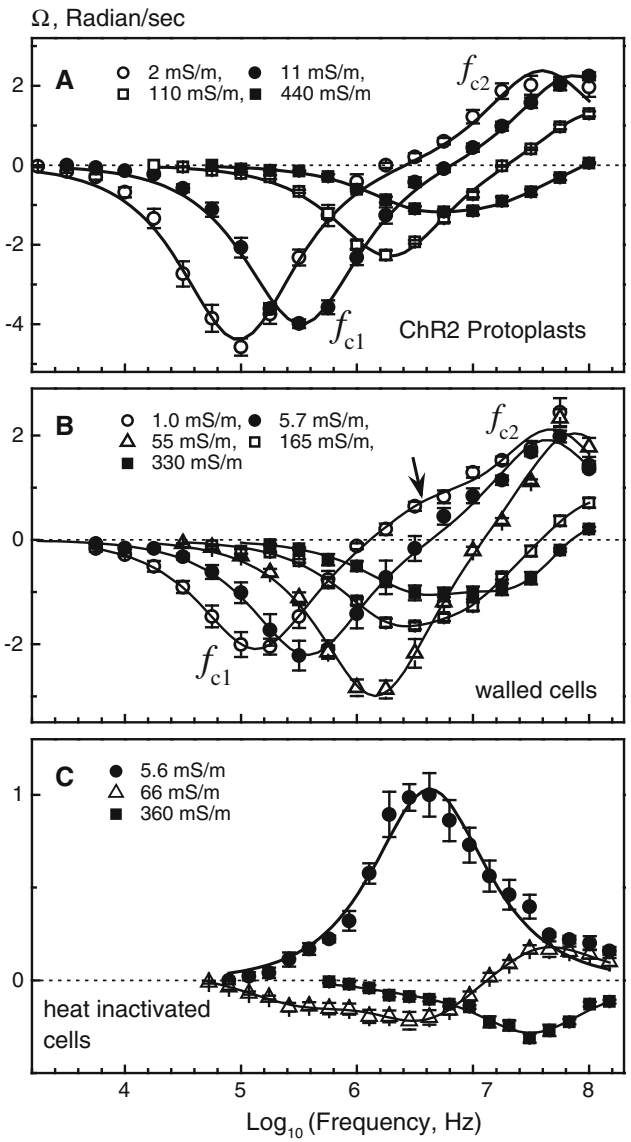

Fig. 2 ROT spectra of various *P. pastoris* samples, including isolated protoplasts (**a**), walled cells (**b**) and heat-inactivated cells (**c**), measured at the indicated external conductivities, σ_e. Each spectrum is the mean (±SE) of five to seven single measurements. Curves are best Lorentzian fits to the data. Peak frequencies f_{c1} and f_{c2} denote the anti- and cofield peaks caused, respectively, by plasma membrane and cytosolic dispersions. **b** *Arrow* points to an additional shoulder in the ROT spectrum of walled cells, at $\sigma_e = 1$ mS/m. As expected, heat-mediated destruction of the plasma membrane completely abolished the antifield ROT peak at low conductivity (**c**, *circles*). For further details see text and the legend to Fig. 3

Fig. 3b, isolated protoplasts displayed two transitions in DEP mobility (f_{d1} and f_{d2}) over a very broad conductivity range (~1–800 mS/m). If field frequency f was $f_{d1} < f < f_{d2}$, the protoplasts were attracted to the electrodes by positive DEP. Otherwise, i.e., for $f < f_{d1}$ and $f > f_{d2}$, the DEP response was negative. The first transition frequency (f_{d1}) increased linearly with conductivity, whereas the high-frequency transition ($f_{d2} \approx 180$ MHz) was largely independent of σ_e. This result in fact confirms recent studies of the second crossover performed on mouse myeloma cells (Chung et al. 2011). At high conductivities ($\sigma_e > \sim 0.8$ S/m), protoplasts showed only negative DEP over the whole frequency range.

Compared to isolated protoplasts (Fig. 3b), the walled cells of *P. pastoris* exhibited a much steeper conductivity dependence of the f_{d1} transition at high and intermediate conductivities ($\sigma_e > 10$ mS/m, Fig. 3d). Moreover, decreasing σ_e below ~10 mS/m completely abolished the DEP transition (f_{d1}) of walled cells (but not of protoplasts) in the kilohertz range. As with the cofield ROT peak f_{c2} (see above), the high-frequency transition f_{d2} was rather insensitive to the presence of the cell wall.

In addition to the complete ROT spectra shown in Fig. 2, we directly analyzed the impact of ChR2 expression on the plasma membrane capacitance (C_m) and conductance (G_m) by means of the CRF technique. This approach permits accurate and rapid measurements of the characteristic frequencies (f_{c1}) of the fastest antifield rotation in large cell samples. Figure 4 summarizes the radius-normalized $f_{c1} \cdot r$ data plotted versus σ_e for isolated protoplasts and walled cells of *P. pastoris*. Open and filled symbols in Fig. 4 denote wt and ChR2-expressing samples, respectively. Given the highly linear relationships between the $f_{c1} \cdot r$ and σ_e observed in all samples of cells and protoplasts (Fig. 4), we applied Eq. 6 ("Appendix" section) to calculate the C_m and G_m values. As seen in Fig. 4a, the least-square fits to the data obtained on wt and ChR2-expressing protoplasts overlap, thus yielding very similar mean C_m values of 7.9 and 8.1 mF/m^2, respectively. The C_m values of walled cells (7.8 and 8.0 mF/m^2) (Fig. 4b) are also comparable to the corresponding data of protoplasts. In contrast, the G_m of walled cells (0.85–0.95 kS/m^2) considerably exceeds that of isolated protoplasts (0.11–0.22 kS/m^2). Comparison of the C_m and G_m values obtained by the CRF technique (Table 1) did not reveal any differences between the wt and ChR2-expressing *P. pastoris* cells (and protoplasts).

Taking the above ROT and DEP data together, ChR2 expression did not cause any significant changes in the AC electrokinetic behavior of *P. pastoris*, including both walled cells and isolated protoplasts. This is particularly evident from the overlapping, filled and empty symbols representing ChR2 and wt samples, respectively, in Figs. 3 and 4. Therefore, the electrokinetic data of wt and ChR2 samples were pooled for further analysis.

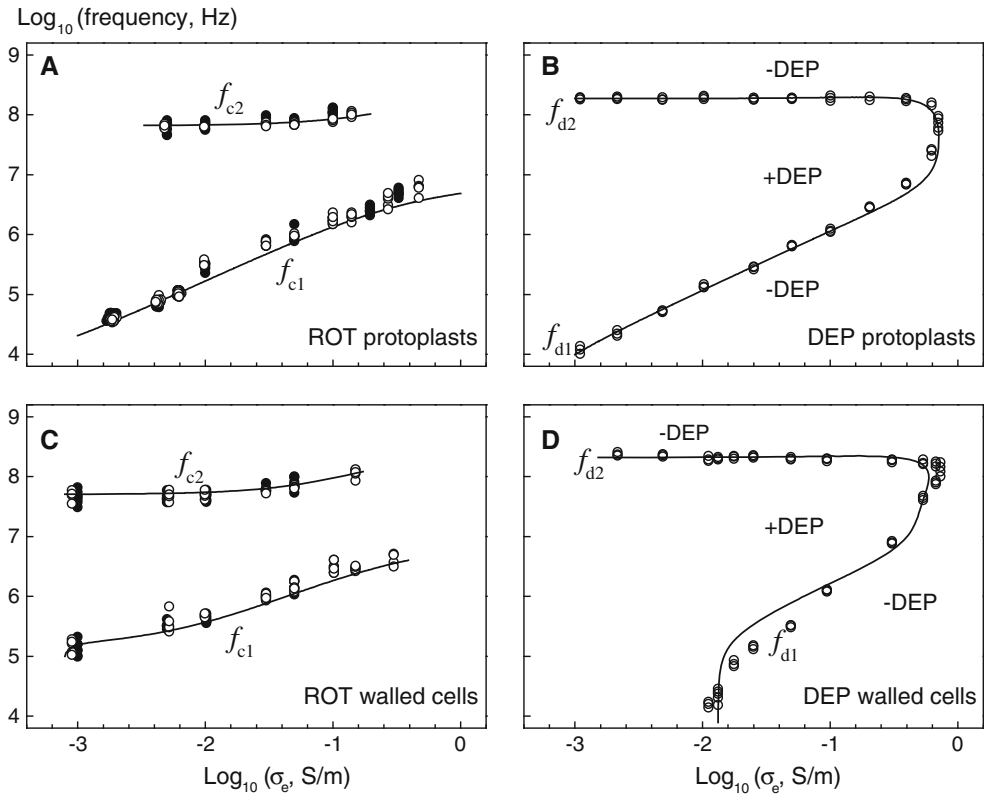

Fig. 3 Conductivity dependencies of the characteristic ROT (**a**, **c**) and DEP (**b**, **d**) frequencies of isolated protoplasts and intact cells of *P. pastoris* (*top* and *bottom rows*, respectively), plotted in double-logarithmic coordinates. Peak frequencies f_{c1} and f_{c2} were derived from the ROT spectra, as shown in Fig. 2. Transition DEP frequencies f_{d1} and f_{d2} were determined in independent experiments. Overlapping *filled* and *empty* symbols (**a**, **c**) denote ChR2-expressing and wt samples, respectively. Curves are best simultaneous fits of the single-shell and double-shell models to the data of protoplasts and walled cells, respectively. The fitted results are listed in Table 1

Dielectric Properties of *P. pastoris* Cells and Protoplasts

The total number of ROT peaks/shoulders indicates the number of dielectric interfaces (or concentric compartments) within a biological particle (Glaser et al. 1983; Fuhr et al. 1985). Given that isolated *P. pastoris* protoplasts exhibited two ROT peaks and walled *P. pastoris* cells showed up to three ROT peaks/shoulders over the entire range of conductivity (Fig. 2a, b), we applied, respectively, the SSM and the DSM to analyze their ROT/DEP responses.

To extract the dielectric properties of protoplasts, we fitted simultaneously the SSM to the experimental ROT and DEP data presented in Fig. 3a, b. The approach used here was to adjust the unknown dielectric parameters (by varying them within realistic ranges) in order to achieve simultaneously subjective best fits of the theoretical curves to ROT and DEP data. For these calculations, the mean radius of protoplasts, $r = 2.6 \pm 0.2$ µm, was found microscopically. The continuous curves in Fig. 3a were generated with the SSM from the points where the derivative of the ROT speed, Ω (combination of Eqs. 3 and 4), with respect to field frequency is zero, i.e., $d\Omega/df = 0$. Table 1 summarizes the best-fit values for C_m, G_m, ε_i and σ_i, which were also used for calculation of the theoretical curve ($Re\chi^* = 0$, see Eqs. 1 and 4) for the crossover frequencies of DEP ($f_{d1,2}$) in Fig. 3b. As evident from Fig. 3a, b, the SSM matches very closely the experimental ROT and DEP data of protoplasts over the entire ranges of field frequency and external conductivity.

The dielectric properties of walled *P. pastoris* cells were derived similarly but with a more complex DSM (see "Appendix" Eq. 7) accounting for the presence of the second, outer dielectric shell (i.e., the yeast cell wall) in addition to the plasma membrane. For calculations, the thickness of the cell wall was assumed to be $d_w = 100$ nm, as determined by electron microscopy elsewhere (Canales et al. 1998). Cell radius $r = 2.1 \pm 0.3$ µm was somewhat smaller than that of isolated protoplasts. Using these geometric data, simultaneous fitting of the DSM to the ROT and DEP data of intact cells (Fig. 3c, d) yielded C_m, ε_i and

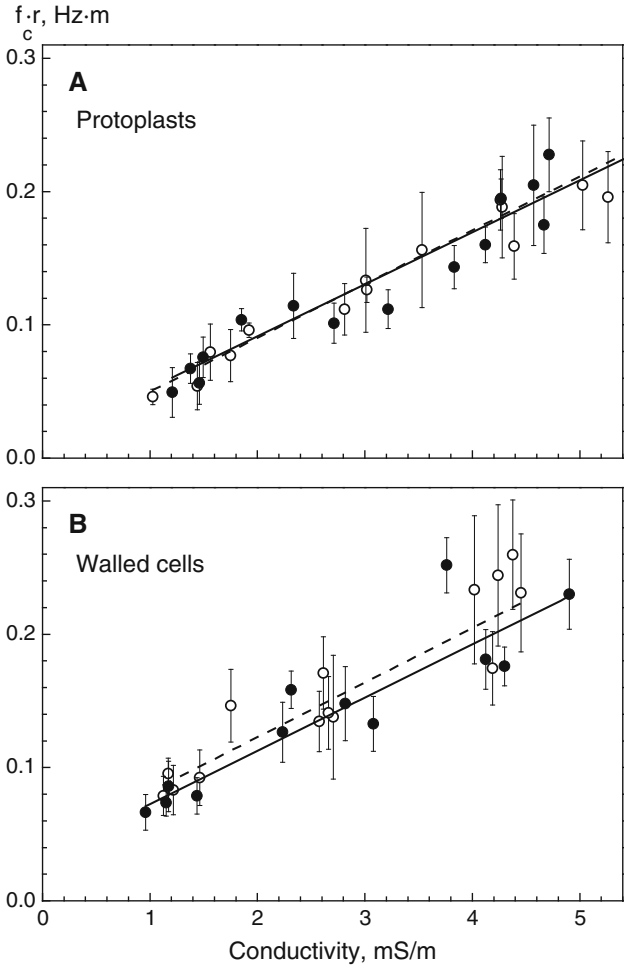

Fig. 4 Determination of the plasma membrane properties of isolated protoplasts (**a**) and intact cells (**b**) of *P. pastoris* by means of the contra-rotating field technique. Plotted are the radius-normalized f_{c1} values ($f_{c1} \cdot r$) versus the external conductivity σ_e. ChR2-expressing and wt samples are given by *filled* and *empty* symbols, respectively. Each data point is the mean ± SD of ~20 individual cells, measured at similar conductivities. Lines are the least-square approximations of Eq. 6 ("Appendix" section) to the data sets, each containing up to 300 cells. *Dashed* and *continuous lines* denote wt and ChR2-expressing samples, respectively. According to Eq. 6, the slope of the fitted line is inversely proportional to the area-specific membrane capacitance C_m, whereas the *y*-intercept is related to the membrane conductance G_m. The line slopes calculated for ChR2-expressing cells and protoplasts are very similar to those of the corresponding wt samples. This implies that protein expression did not alter significantly the C_m of *P. pastoris*. The fitted C_m and G_m values are summarized in Table 1

σ_i values which were very similar to the corresponding data of protoplasts (Table 1). In contrast, the DSM-based G_m value of 5 kS/cm^2 in intact cells exceeded by far the G_m = 0.2–0.4 kS/cm^2 calculated for wall-less protoplasts with the SSM (see discussion below). The permittivity of the cell wall was relatively low, $\varepsilon_w \approx 20 \cdot \varepsilon_0$, suggesting high content of low-polarity compounds. Accordingly, the poor conductivity $\sigma_w \approx 0.06$ S/m, calculated with the DSM, implies low ionic concentration in the cell wall.

As already mentioned, the combined ROT and DEP analysis presented in Figs. 2, 3, and 4 did not reveal any influence of ChR2 expression on the dielectric properties of *P. pastoris* cells and protoplasts. Small differences in G_m between wt and ChR2 cells/protoplasts detected by the CRF technique (Fig. 4) did not reach statistical significance. Although ROT and DEP seemed so far incapable of resolving ChR2-mediated changes in the electrical properties of *P. pastoris*, the above dielectric analysis was essential for establishing efficient electrofusion protocols for production of giant *P. pastoris* protoplasts suitable for electrophysiological measurements (see next section).

Optimization of Multi-cell Electrofusion

Electrofusion of cells involves two major steps (Zimmermann and Neil 1996; Usaj et al. 2010; Gabrijel et al. 2009; Sukhorukov et al. 2005). First, application of a nonuniform AC field to a cell suspension aligns the cells by DEP into chains along the field lines, thus producing tight membrane contacts between cells. For multi-cell electrofusion (MCE), high cell densities are used to generate numerous chains in close contact. Second, a train of high-intensity DC pulses is applied to induce membrane breakdown in the contact zones, which initiates fusion of adjacent cells. MCE requires supracritical DC pulses, at which membrane breakdown occurs not only in the contact zones of cells within a chain but also in the contact zones of cells from neighboring chains.

A phenomenon that can compromise electrofusion by destabilizing or even disrupting protoplast chains is multicell rotation (MCR) (Holzapfel et al. 1982). MCR is caused by local rotating fields due to the superposition of the imposed field E_0 and secondary electric fields from the induced dipoles μ_C within adjacent cells. Figure 5 shows theoretical DEP and MCR spectra of *P. pastoris* protoplasts calculated with the dielectric data given in Table 1 for electrofusion conditions ($\sigma_e \approx 80$ µS/cm). As evident from Fig. 5, protoplasts experienced only positive DEP force but virtually no torque via the MCR mechanism, within a frequency range of ~1 to ~10 MHz. In order to fully avoid MCR, we used an AC field of 2 MHz, which gave rise to rapid collection and stable alignment of protoplasts into chains by DEP.

Since *P. pastoris* protoplasts are small enough to undergo Brownian motion, the protoplast chains can break

Table 1 Dielectric properties of intact cells and isolated protoplasts of *P. pastoris* determined by the contra-rotating field (CRF) technique, combined ROT and DEP measurements and patch clamp

	Technique	Model used	Cytosol		Plasma membrane		Cell wall		*N*
			ε_i (F/m)	σ_i (S/m)	C_m (mF/m^2)	G_m (kS/m^2)	ε_w (F/m)	σ_w (S/m)	
wt protoplasts	CRF	SSM			7.9 ± 0.4	0.22 ± 0.10			300
ChR2 protoplasts	CRF	SSM			8.1 ± 0.6	0.11 ± 0.09			300
Walled wt cells	CRF	SSM			7.8 ± 0.8	0.85 ± 0.18			260
Walled ChR2 cells	CRF	SSM			8.0 ± 1.0	0.95 ± 0.17			260
wt and ChR2 protoplasts	ROT + DEP	SSM	$60\cdot\varepsilon_0$	0.75	7.4	0.2			230
Walled wt and ChR2 cells	ROT + DEP	DSM	$70\cdot\varepsilon_0$	1.00	8.0	5.0	$20\cdot\varepsilon_0$	0.06	200
Protoplasts	Patch clamp				7.5 ± 1.5	$(8 \pm 4) \cdot 10^{-3}$			10

The mean (±SD) radii of cells and protoplasts were $r_C = 2.01 \pm 0.29$ and $r_P = 2.55 \pm 0.23$ µm, respectively. Radii were determined during CRF, ROT and DEP measurements with a calibrated ocular micrometer. The thickness of the cell wall ($d_w \approx 100$ nm) has been reported elsewhere (Canales et al. 1998). Models used for calculations were the single-shell model (SSM) and the double-shell model (DSM). Lines 5 and 6 (combined ROT and DEP measurements) contain the dielectric data of protoplasts and cells used, for calculation of the fitted curves in Fig. 3

apart when the DEP force is switched off, e.g., during the time lag between AC and pulsing DC fields (usually denoted as the alignment off time [AOT] in the literature). Using an arbitrary waveform generator (see Materials and Methods), we greatly reduced the AOT to 1 µs compared to the AOTs of 10–100 ms delivered by most commercial electrofusion devices. The reduction of AOT was essential to provide for a sufficiently tight contact between protoplasts during application of DC pulses triggering electrofusion.

The generation of membrane breakdown in the contact zones of aligned cells is a further crucial step of electrofusion. The critical field strength (E_{crit}) required for breakdown at membrane sites facing the electrodes ($\cos\theta = 1$) can be estimated as $E_{crit} = V_{crit}/(1.5 \cdot r)$, where $V_{crit} = 1$ V is the breakdown voltage. Using a mean radius value of ~2.6 µm, an E_{crit} value of ~2.6 kV/cm was obtained for isolated *Pichia* protoplasts. Based on observations that the most favorable field strength of breakdown pulses is two to four times E_{crit} (Zimmermann and Neil 1996), the following experiments were restricted to the field strength ranging between 8 and 11 kV/cm.

In addition to the field strength, the optimal duration of DC pulses is dictated by the time constant of membrane charging, τ_m. The τ_m value can be estimated directly from the ROT spectrum of protoplasts measured in electrofusion medium (Fig. 2), using the relation $\tau_m = (2\pi f_{c1})^{-1} \approx 1$ µs (Sukhorukov et al. 2006). To achieve the stationary level of the induced membrane voltage, V_g, the duration of breakdown pulses was set to ~20 µs.

The above considerations show that detailed dielectric analysis of parental *Pichia* protoplasts allows rapid optimization of several field parameters most critical for electrofusion. The improved protocol regularly resulted in multiple fusion events, yielding giant yeast protoplasts with a diameter of up to 35 µm (Fig. 6b; Supplemental Fig. S3). In wt yeasts, the portion of parental protoplasts involved in the fusion process reached 50–60 %. The fusion yield obtained with ChR2-expressing protoplasts was somewhat lower (10–20 %).

Patch Clamp of Electrofused Protoplasts

Electrofused ChR2 protoplasts with a diameter of ~30 µm, as shown in Fig. 6b, were best suited for patch clamp experiments. In patch clamp experiments, giant *P. pastoris* protoplasts formed gigaseals with resistances of >1 GΩ in cell-attached configuration within 10–15 min. Seal-promoting solutions contained high calcium concentration. The use of potassium- and EGTA-free pipette solution also supported the sealing process. The whole-cell configuration was achieved routinely by applying slight transient suction through the patch pipette. Linear regression of the whole-cell capacitance (C_C, [pF]) data plotted versus the membrane area of giant protoplasts (for cell diameters ranging 10–33 µm) yielded a value for the area-specific membrane capacitance of $C_m = 7.5 \pm 1.5$ mF/m^2 (Fig. 6b, $n = 10$). This C_m value matches well that of parental protoplasts, derived from the combined ROT and DEP experiments (Table 1). This also means that the entire cytoplasmic membrane of fused protoplasts was fully accessible to the patch pipette.

Although the patch clamp and CRF techniques gave consistent C_m values for giant and parental protoplasts, the

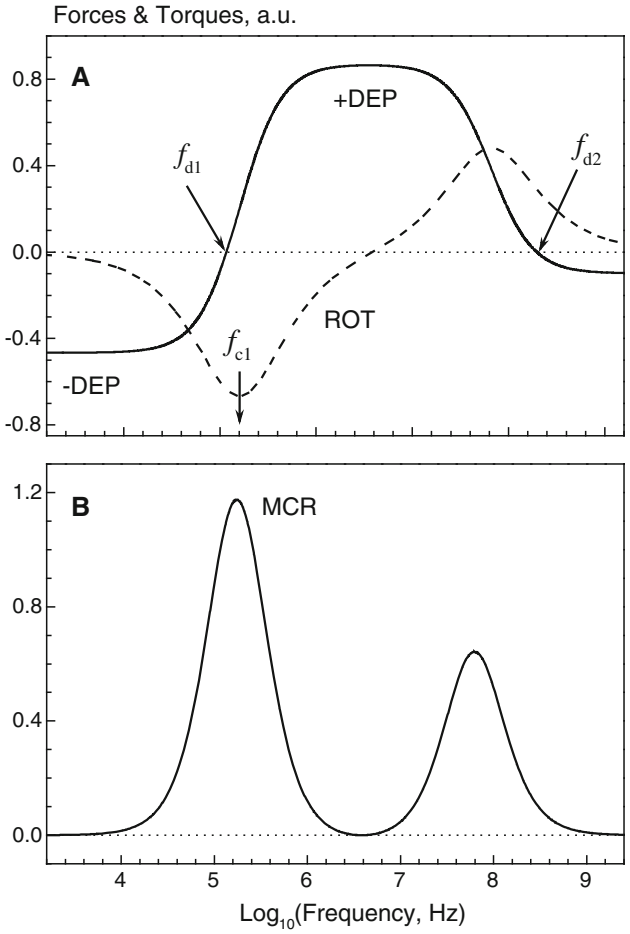

Fig. 5 Theoretical ROT, DEP (**a**) and MCR (**b**) spectra calculated with the single-shell model (see "Appendix" section), using the dielectric data of isolated protoplasts given in Table 1 and the external conductivity $\sigma_e = 10$ mS/m of the electrofusion medium. The ROT and DEP responses are proportional, respectively, to the imaginary and real parts (Eqs. 1, 3) of the complex polarizability χ^* (Eq. 4). The MCR spectrum was calculated as $Im^2\chi^*/(4 - Re\chi^*)$ (Eq. 2). Within a frequency range of 1–10 MHz, protoplasts experience the highest DEP force but a negligible torque via the MCR mechanism. These frequencies are therefore best suited for protoplast alignment by DEP during electrofusion

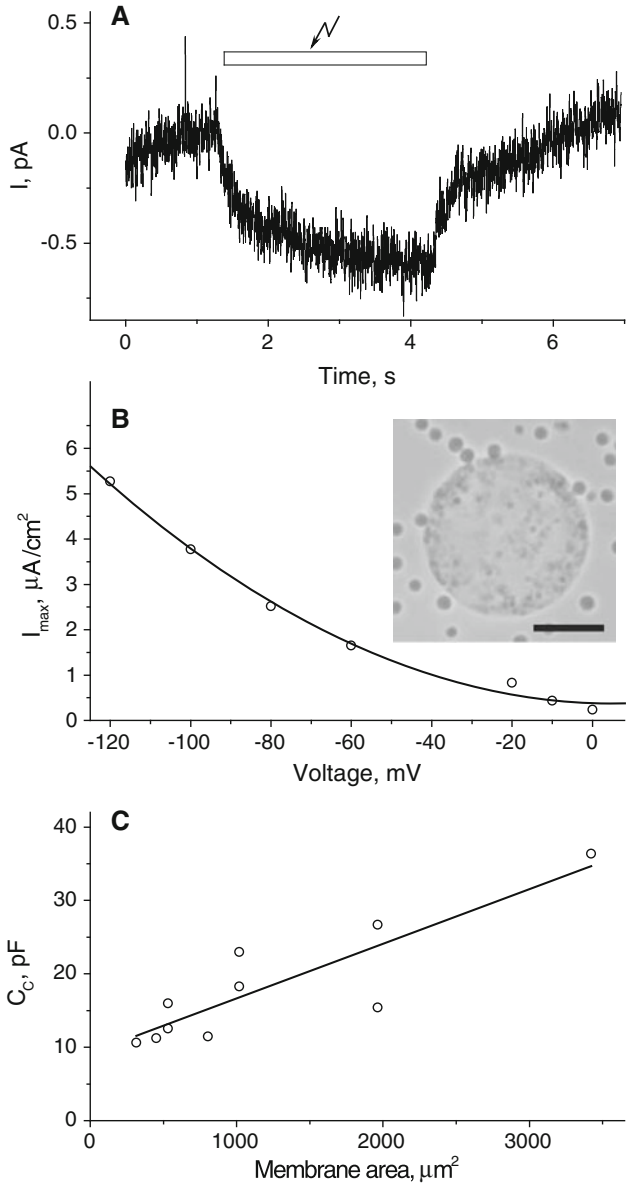

Fig. 6 Typical whole-cell patch clamp recording (**a**) from a giant protoplast of *P. pastoris* expressing ChR2(C128T)-YFP upon illumination with blue light (*white bar*) at zero holding potential. The corresponding *I–V* relationship is shown in **b**. *Inset* in **b** shows a microphotograph of a typical giant protoplast produced by multi-cell electrofusion (*bar* = 10 µm). **c** Cumulative plot of cell capacitance (C_C, pF) versus the membrane area of electrofused giant protoplasts. Linear regression of the data yields a slope of 7.5 ± 0.15 µF/cm² and a *y*-intercept of 9.66 ± 0.33 pF, representing the area-specific membrane capacitance, C_m, and the stray capacitance, respectively. The C_m value of giant protoplasts determined by patch clamp is in good agreement with the corresponding data of tiny parental protoplasts, measured by ROT and DEP. The stray capacitance also matches well with the value measured in control experiments using lipid-clogged patch pipettes

area-specific membrane conductance, G_m, obtained by the CRF technique for tiny parental protoplasts exceeded by far the G_m of giant protoplasts measured by patch clamp (Table 1). The discrepancy can be attributed to the effect of the tangential surface conductance, K_S, which is known to increase the effective conductance of microscopic cells and particles by a radius-dependent factor (for schematic representation see p. 231 in Jones 1995). As pointed out elsewhere (Sukhorukov et al. 1993), the effect of the

tangential ion currents has to be added to the radial, transmembrane conductivity ($G_{m,trans}$) to an extent which increases heavily with decreasing cell radius: $G_m = G_{m,trans} + 2K_S/r^2$. Given that the patch clamp technique yields only the transmembrane conductance $G_{m,trans} \approx 8$ S/m^2, the large effective $G_m \approx 110$–220 S/m^2 of tiny parental protoplasts measured by CRF is apparently dominated by the surface conductance effect. A further source for the discrepancy may be the adoption of the low frequency (DC) approximation in Eq. 6 used for the evaluation of G_m from the CRF data (Fig. 4a). This issue has recently been considered in detail by Lei et al. (2011). In walled *P. pastoris* cells, an additional ion-rich layer (e.g., the thin periplasmic space between the plasma membrane and the cell wall [Hölzel 1997]) can also contribute to the surface conductance, thus increasing markedly their effective membrane conductance ($\sim$1–5 kS/m^2, Table 1).

Although our patch clamp experiments failed to reveal any light-activated currents in the small-sized parental protoplasts prepared from ChR2-expressing *P. pastoris* cells, some electrofused giant protoplasts showed readily detectable photocurrents upon illumination with blue light, as seen in Fig. 6c (in addition to the dark conductance G_m mentioned above). The kinetics of the inwardly directed photocurrent in giant *P. pastoris* protoplasts was typical for the mutant C128T of ChR2 (Berndt et al. 2009) exhibiting the characteristic slow closing time constant. Other ChR2-expressing eukaryotic cells, including *Xenopus* oocytes, HEK293 cells and *S. cerevisiae*, exhibit similar photocurrent kinetics upon light excitation (Berndt et al. 2009), which implies full functionality of the light-activated cation channel ChR2 in electrofused protoplasts of *P. pastoris* (Fig. 6). Compared to the above eukaryotic systems, however, the ChR2-mediated photocurrent in giant *P. pastoris* protoplasts showed much smaller amplitudes (Fig. 6), which can be attributed to the relatively low density of ChR2 protein in the plasma membrane, revealed by fluorescence microscopy (Fig. 1c).

Conclusion

This and early studies (Arnold et al. 1986; Huang et al. 1992; Zhou et al. 1996) have shown that ROT, DEP and related AC electrokinetic techniques provide powerful experimental tools for analyzing the dielectric structure of yeast cells and protoplasts with single-cell resolution. Besides their importance for many applications in microfluidic devices (for review see Pethig 2010; Gagnon 2011), the dielectric data of *P. pastoris* obtained here may also be useful for the interpretation of impedance measurements of yeast cultures, which are routinely used in microbial biotechnology for online monitoring of the biomass, cell division and metabolism during fermentation in bioreactors (Yardley et al. 2000; Asami and Yonezawa 1996; Kiviharju et al. 2008).

Based on the dielectric analysis of parental cells and protoplasts, we developed an efficient protocol for generation of stable multinucleated *P. pastoris* protoplasts by means of electrofusion. Due to the manifold extension of the plasma membrane area in giant protoplasts over that of parental cells, direct electric access could be readily established to the light-activated cation channel ChR2, expressed heterologously in *P. pastoris*. Although this study focuses on the patch clamp recording of ChR2, the approach presented here can be generally applied for the functional analysis of other recombinant channels and transporters, using available, highly efficient *P. pastoris* strains for the production of selected target proteins.

Acknowledgments We thank C. Bamann (MPI of Biophysics) for generously providing us with the *P. pastoris* ChR2(C128T)YFP strain, M. Heidbreder (University of Würzburg) for support with LSM imaging, A. Pustlauck and E. Kaindl (MPI of Biophysics) for technical support and J. Reichert (MPI of Biophysics), A. Gessner and M. Behringer (University of Würzburg) for construction of electrofusion chambers.

Appendix

Dielectric Models

When exposed to an AC electric field, cells experience mechanical forces, pressures and torques based on the electrostatic interactions of the induced cell dipole with the applied field. The cell dipole (μ) is proportional to the applied field (E_0) and the complex dielectric polarizability of the cell: χ^* ($\mu \propto E_0 \cdot \chi^*$). Among a variety of AC electrokinetic phenomena, dielectrophoresis (DEP) and multi-cell rotation (MCR) are most critical for electrofusion. Thus, cell alignment by positive DEP is required to produce stable cell chains prior to fusion, whereas the MCR effect may lead to destabilization or even to disruption of cell chains.

Exerted by an inhomogeneous field, the dielectrophoretic force (F_{DEP}) is proportional to the cell volume V ($\propto r^3$, with r = cell radius), the field gradient ∇E_0 and the real part of polarizability χ^* (Jones 1995):

$$F_{DEP} = 2\pi r^3 \varepsilon_e \nabla E_0^2 Re\chi^* \quad (1)$$

In addition to the DEP force, MCR can occur in a linear AC field if cell chains are misaligned with respect to the field, E_0 (Holzapfel et al. 1982). In case of two adjacent cells, the following relation holds for the frequency-dependent MCR speed, Ω_{MCR}:

$$\Omega_{MCR} = \frac{3\varepsilon_e}{8\eta} E_0^2 \sin 2\theta \frac{\mathrm{Im}^2\chi^*}{4 - \mathrm{Re}\chi^*} \quad (2)$$

where θ is the angle between the field E_0 and the line connecting the centers of the two cells and η is the viscosity of the suspending medium.

In a rotating field, the cell rotation, Ω_{ROT}, is determined by the imaginary part of χ^*:

$$\Omega_{ROT} = -\frac{\varepsilon_e E_0^2}{2\eta} \mathrm{Im}\ \chi^* \quad (3)$$

As evident from Eqs. 1–3, DEP, MCR and ROT are interrelated phenomena linked to each other through the complex polarizability (χ^*), which in turn depends on the dielectric cell structure. Using an approach described elsewhere (Jones 1995), we derived mathematical expressions for the χ^* of single- and double-shelled dielectric particles.

In the present study, the ROT and DEP responses of isolated protoplasts of *P. pastoris* could be approximated quite well with the single-shell model (SSM). Given that the protoplast radii ($r \approx 2$ µm) are much larger than the thickness of the plasma membrane (~ 10 nm), a simplified expression of the complex polarizability (χ^*) was used:

$$\chi^* = \frac{r\, C_m^* \left(\varepsilon_i^* - \varepsilon_e^*\right) - \varepsilon_i^* \varepsilon_e^*}{r\, C_m^* \left(\varepsilon_i^* + 2\varepsilon_e^*\right) + 2\varepsilon_i^* \varepsilon_e^*} \quad (4)$$

where the complex permittivity (ε^*) is defined as $\varepsilon^* = \varepsilon - \mathrm{j}\sigma/\omega$, with ε as the real permittivity (F/m) and σ as the conductivity (S/m) of the medium (subscript "e") and cytosol (subscript "i"); $\mathrm{j} = (-1)^{1/2}$; and $\omega = 2\pi f$ is the radian field frequency. The complex area-specific membrane capacitance is given by $C_m^* = C_m - \mathrm{j}\, G_m/\omega$, where C_m (F/m^2) and G_m (S/m^2) are the real membrane capacitance and conductance per unit area, respectively.

The ROT spectra of single-shelled cells can also be presented as a superposition of two Lorentzian peaks:

$$\Omega(f) = 2A_1 \frac{(f/f_{c1})}{1 + (f/f_{c1})^2} + 2A_2 \frac{(f/f_{c2})}{1 + (f/f_{c2})^2} \quad (5)$$

where A_1 and A_2 are the amplitudes of the anti- and cofield peaks centered at f_{c1} and f_{c2}, respectively. Equation 5 was used for to determine the f_{c1} and f_{c2} values from the ROT spectra, as shown in Fig. 2a.

Provided that $\sigma_i \gg \sigma_e \gg \sigma_m$, the SSM yields the following relationship between the f_{c1}, radius r, σ_e and membrane properties:

$$f_{c1} \cdot r = \frac{\sigma_e}{\pi \cdot C_m} + \frac{r \cdot G_m}{2\pi \cdot C_m} \quad (6)$$

Equation 6 was used in this study to determine the C_m and G_m values from the f_{c1} data obtained by the CRF technique.

The double-shell model (DSM), applied here to walled *P. pastoris* cells, yields the following expression for complex polarizability (χ^*):

$$\chi^* = \frac{C_m^* r\left(\varepsilon_w^*\left((a^3+2)\varepsilon_i^* + 2(a^3-1)\varepsilon_w^*\right) - \varepsilon_e^*\left((a^3-1)\varepsilon_i^* + (2a^3+1)\varepsilon_w^*\right)\right) - a\varepsilon_i^*\varepsilon_w^*\left((2a^3+1)\varepsilon_e^* - 2(a^3-1)\varepsilon_w^*\right)}{C_m^* r\left(2\varepsilon_e^*\left((a^3-1)\varepsilon_i^* + (2a^3+1)\varepsilon_w^*\right) + \varepsilon_w^*\left((a^3+2)\varepsilon_i^* + 2(a^3-1)\varepsilon_w^*\right)\right) + 2a\varepsilon_i^*\varepsilon_w^*\left((2a^3+1)\varepsilon_e^* + (a^3-1)\varepsilon_w^*\right)} \quad (7)$$

where $a = r/(r - d)$, with r and d denoting the cell radius and the thickness of the cell wall, respectively. Subscript "w" refers to the cell wall. The meaning of other symbols is the same as in Eqs. 1–6.

References

Arnold WM, Zimmermann U (1988) Electro-rotation—development of a technique for dielectric measurements on individual cells and particles. J Electrostat 21:151–191

Arnold WM, Geier BM, Wendt B, Zimmermann U (1986) The change in the electrorotation of yeast cells effected by silver ions. Biochim Biophys Acta 889:35–48

Asami K, Yonezawa T (1996) Dielectric behavior of wild-type yeast and vacuole-deficient mutant over a frequency range of 10 kHz to 10 GHz. Biophys J 71:2192–2200

Bamann C, Kirsch T, Nagel G, Bamberg E (2008) Spectral characteristics of the photocycle of channelrhodopsin-2 and its implication for channel function. J Mol Biol 375:686–694

Berndt A, Yizhar O, Gunaydin LA, Hegemann P, Deisseroth K (2009) Bi-stable neural state switches. Nat Neurosci 12:229–234

Bretthauer RK, Castellino FJ (1999) Glycosylation of *Pichia pastoris*–derived proteins. Biotechnol Appl Biochem 30:193–200

Canales M, Buxado JA, Heynngnezz L, Enriquez A (1998) Mechanical disruption of *Pichia pastoris* yeast to recover the recombinant glycoprotein Bm86. Enzyme Microb Technol 23:58–63

Chung C, Waterfall M, Pells S, Menachery A, Smith S, Pethig R (2011) Dielectrophoretic characterisation of mammalian cells above 100 MHz. J Electr Bioimp 2:64–71

Cregg JM, Barringer KJ, Hessler AY, Madden KR (1985) *Pichia pastoris* as a host system for transformations. Mol Cell Biol 5:3376–3385

Daly R, Hearn MTW (2005) Expression of heterologous proteins in *Pichia pastoris*: a useful experimental tool in protein engineering and production. J Mol Recognit 18:119–138

De Schutter K, Lin YC, Tiels P, Van Hecke A, Glinka S, Weber-Lehmann J, Rouze P, Van de Peer Y, Callewaert N (2009) Genome sequence of the recombinant protein production host *Pichia pastoris*. Nat Biotechnol 27:561–566

Diatloff E, Forde BG, Roberts SK (2006) Expression and transport characterisation of the wheat low-affinity cation transporter (LCT1) in the methylotrophic yeast *Pichia pastoris*. Biochem Biophys Res Commun 344:807–813

Fuhr G, Gimsa J, Glaser R (1985) Interpretation of electrorotation of protoplasts. 1 Theoretical considerations. Studia Biophys 108:149–164

Gabrijel M, Bergant M, Kreft M, Jeras M, Zorec R (2009) Fused late endocytic compartments and immunostimulatory capacity of dendritic-tumor cell hybridomas. J Membr Biol 229:11–18

Gagnon ZR (2011) Cellular dielectrophoresis: applications to the characterization, manipulation, separation and patterning of cells. Electrophoresis 32:2466–2487

Gimsa J, Müller T, Schnelle T, Fuhr G (1996) Dielectric spectroscopy of single human erythrocytes at physiological ionic strength: dispersion of the cytoplasm. Biophys J 71:495–506

Glaser R, Fuhr G, Gimsa J (1983) Rotation of erythrocytes, plant-cells, and protoplasts in an outside rotating electric-field. Studia Biophys 96:11–20

Holzapfel C, Vienken J, Zimmermann U (1982) Rotation of cells in an alternating electric field theory and experimental proof. J Membr Biol 67:13–26

Hölzel R (1997) Electrorotation of single yeast cells at frequencies between 100 Hz and 1.6 GHz. Biophys J 73:1103–1109

Huang Y, Hölzel R, Pethig R, Wang XB (1992) Differences in the AC electrodynamics of viable and non-viable yeast cells determined through combined dielectrophoresis and electrorotation studies. Phys Med Biol 37:1499–1517

Jones TB (1995) Electromechanics of particles. Cambridge University Press, Cambridge

Kiesel M, Reuss R, Endter J, Zimmermann D, Zimmermann H, Shirakashi R, Bamberg E, Zimmermann U, Sukhorukov VL (2006) Swelling-activated pathways in human T-lymphocytes studied by cell volumetry and electrorotation. Biophys J 90:4720–4729

Kiviharju K, Salonen K, Moilanen U, Eerikäinen T (2008) Biomass measurement online: the performance of in situ measurements and software sensors. J Ind Microbiol Biotechnol 35:657–665

Klinner U, Böttcher F, Samsonova IA (1980) Hybridization of *Pichia guilliermondii* by protoplast fusion. In: Ferenczy L, Farkas GL (eds) Advances in protoplast research. In: Proceedings of the 5th international protoplast symposium. Akadémiai Kiadó, Budapest, pp 113–118

Lei U, Sun P-H, Pethig R (2011) Refinement of the theory for extracting cell dielectric properties from dielectrophoresis and electrorotation experiments. Biomicrofluidics 5:044109

Macauley-Patrick S, Fazenda ML, McNeil B, Harvey LM (2005) Heterologous protein production using the *Pichia pastoris* expression system. Yeast 22:249–270

Pethig R (2010) Dielectrophoresis: status of the theory, technology, and applications. Biomicrofluidics 4:022811

Priel A, Gil Z, Moy VT, Magleby KL, Silberberg SD (2007) Ionic requirements for membrane-glass adhesion and giga seal formation in patch-clamp recording. Biophys J 92:3893–3900

Sukhorukov VL, Arnold WM, Zimmermann U (1993) Hypotonically induced changes in the plasma-membrane of cultured mammalian cells. J Membr Biol 132:27–40

Sukhorukov VL, Reuss R, Zimmermann D, Held C, Müller KJ, Kiesel M, Gessner P, Steinbach A, Schenk WA, Bamberg E, Zimmermann U (2005) Surviving high-intensity field pulses: strategies for improving robustness and performance of electrotransfection and electrofusion. J Membr Biol 206:187–201

Sukhorukov VL, Reuss R, Endter JM, Fehrmann S, Katsen-Globa A, Gessner P, Steinbach A, Müller KJ, Karpas A, Zimmermann U, Zimmermann H (2006) A biophysical approach to the optimisation of dendritic-tumour cell electrofusion. Biochem Biophys Res Commun 346:829–839

Terpitz U, Raimunda D, Westhoff M, Sukhorukov VL, Beauge L, Bamberg E, Zimmermann D (2008) Electrofused giant protoplasts of *Saccharomyces cerevisiae* as a novel system for electrophysiological studies on membrane proteins. Biochim Biophys Acta 1778:1493–1500

Tschopp JF, Brust PF, Cregg JM, Stillman CA, Gingeras TR (1987) Expression of the *lacZ* gene from two methanol-regulated promoters in *Pichia pastoris*. Nucleic Acids Res 15:3859–3876

Usaj M, Trontelj K, Miklavcic D, Kanduser M (2010) Cell–cell electrofusion: optimization of electric field amplitude and hypotonic treatment for mouse melanoma (B16–F1) and Chinese hamster ovary (CHO) cells. J Membr Biol 236:107–116

Yardley YE, Kell DB, Barrett J, Davey CL (2000) On-line, real-time measurements of cellular biomass using dielectric spectroscopy. Biotechnol Genet Eng Rev 17:3–35

Zhou XF, Markx GH, Pethig R (1996) Effect of biocide concentration on electrorotation spectra of yeast cells. Biochim Biophys Acta 1281:60–64

Zimmermann U, Neil GA (1996) Electromanipulation of cells. CRC Press, Boca Raton

Zimmermann D, Terpitz U, Zhou A, Reuss R, Müller KJ, Sukhorukov VL, Gessner P, Nagel G, Zimmermann U, Bamberg E (2006) Biophysical characterisation of electrofused giant HEK293-cells as a novel electrophysiological expression system. Biochem Biophys Res Commun 348:673–681

Zimmermann D, Zhou A, Kiesel M, Feldbauer K, Terpitz U, Haase W, Schneider-Hohendorf T, Bamberg E, Sukhorukov VL (2008) Effects on capacitance by overexpression of membrane proteins. Biochem Biophys Res Commun 369:1022–1026